© 2020. Published by The Company of Biologists Ltd | Journal of Cell Science (2021) 134, jcs233775. doi:10.1242/jcs.233775

RESEARCH ARTICLE

SPECIAL ISSUE: CELL BIOLOGY OF HOST–PATHOGEN INTERACTIONS

A function of profilin in force generation during malaria parasite motility that is independent of actin binding

Catherine A. Moreau[1,*], Katharina A. Quadt[1,2,§], Henni Piirainen[3,§], Hirdesh Kumar[1,4,5,§], Saligram P. Bhargav[1,3], Léanne Strauss[1,‡], Niraj H. Tolia[4], Rebecca C. Wade[5,6], Joachim P. Spatz[2], Inari Kursula[3,7] and Friedrich Frischknecht[1,¶]

ABSTRACT

During transmission of malaria-causing parasites from mosquito to mammal, *Plasmodium* sporozoites migrate at high speed within the skin to access the bloodstream and infect the liver. This unusual gliding motility is based on retrograde flow of membrane proteins and highly dynamic actin filaments that provide short tracks for a myosin motor. Using laser tweezers and parasite mutants, we previously suggested that actin filaments form macromolecular complexes with plasma membrane-spanning adhesins to generate force during migration. Mutations in the actin-binding region of profilin, a near ubiquitous actin-binding protein, revealed that loss of actin binding also correlates with loss of force production and motility. Here, we show that different mutations in profilin, that do not affect actin binding *in vitro*, still generate lower force during *Plasmodium* sporozoite migration. Lower force generation inversely correlates with increased retrograde flow suggesting that, like in mammalian cells, the slow down of flow to generate force is the key underlying principle governing *Plasmodium* gliding motility.

KEY WORDS: Optical tweezers, Gliding motility, Malaria, *Plasmodium*, Sporozoite, Profilin, Cell motility

INTRODUCTION

Actin filament formation and turnover are key to many cellular processes, including cell motility, and are hence regulated by many different actin-binding proteins. Profilin is a key actin-binding protein in most eukaryotic cells. Mammalian profilins are an important factor regulating actin polymerization by binding to monomeric actin and promoting the exchange of ADP for ATP, which renders monomeric actin ready for incorporation into filaments (Courtemanche and Pollard, 2013). Profilin from *Plasmodium falciparum* (*P. falciparum*; *Pf*) and *Toxoplasma gondii* (*T. gondii*; *Tg*), two members of the protozoan phylum of Apicomplexa also appears to be important for sequestering actin monomers *in vitro* (Skillman et al., 2012; Kursula et al., 2008). Sequestration of actin monomers limits actin polymerization and is important in these single-celled parasites (Mehta and Sibley, 2011; Moreau et al., 2017). Interestingly, apicomplexan profilins contain additional motifs compared to canonical profilins (Kursula et al., 2008; Bhargav et al., 2015). One of these motifs is a β-hairpin arm that contacts the actin monomer and contributes to actin binding (Kursula et al., 2008; Moreau et al., 2017). A second additional motif, investigated in this report, is an acidic loop region that differs among apicomplexan species.

In *Plasmodium*, actin polymerization is important at all stages along the complex life cycle that need motility (Douglas et al., 2015). Several extracellular forms of the parasite rely on a form of motility called gliding, during which the parasites move without changing their shape (Heintzelman, 2015) (Fig. 1). While some forms (ookinetes) move at speeds that are comparable to those for neutrophil migration, others (sporozoites) move over ten times faster, reaching speed peaks of several micrometers per second. In order to achieve this fast speed, the parasite relies on short and highly dynamic actin filaments (Douglas et al., 2018). *Plasmodium* sporozoites are the forms transmitted by the mosquito (Frischknecht and Matuschewski, 2017). They form in parasitic oocysts at the midgut wall of the mosquito and need to be motile to egress from these to the circulating hemolymph (Klug and Frischknecht, 2017). After floating in the hemolymph (Frischknecht et al., 2006), they actively enter into salivary glands, to colonize the salivary ducts (Pimenta et al., 1994; Sultan et al., 1997; Frischknecht et al., 2004). During a mosquito bite, sporozoites are deposited in the dermis where they actively migrate at 1–2 µm/s to search and enter blood capillaries or lymphatic vessels (Amino et al., 2008, 2006; Hopp et al., 2015; Ménard et al., 2013). Those entering the blood will ultimately cross the endothelium in the liver to differentiate within hepatocytes into thousands of red blood-cell infecting merozoites (Tavares et al., 2013; Prudêncio et al., 2006).

Plasmodium sporozoites rely on an actin-myosin motor that resides in the narrow space between the plasma membrane and the subtending inner membrane complex (IMC; Fig. 1). The IMC corresponds to the alveoli, the eponymous organelle of the alveolates, the superphylum that contains the Apicomplexa. As illustrated in Fig. 1, short actin filaments are likely to be formed by a formin localized at the tip of the cell (Douglas et al., 2018). Myosin is anchored to the IMC and at least partially provides the force needed for motility (Meissner et al., 2013, 2002; Bergman et al., 2003; Andenmatten et al., 2013). Myosin also translocates actin

[1]Integrative Parasitology, Center for Infectious Diseases, Heidelberg University Medical School, Im Neuenheimer Feld 324, 69120 Heidelberg, Germany. [2]Department of Cellular Biophysics, Max Planck Institute for Medical Research and Laboratory of Biophysical Chemistry, Heidelberg University, Jahnstrasse 29, 69120 Heidelberg, Germany. [3]Biocenter Oulu and Faculty of Biochemistry and Molecular Medicine, University of Oulu, Aapistie 7, 90220 Oulu, Finland. [4]Department of Molecular Microbiology, Washington University School of Medicine, St Louis, MO 63110, USA. [5]Center for Molecular Biology (ZMBH), DKFZ-ZMBH Alliance and Interdisciplinary Center for Scientific Computing (IWR), Heidelberg University, Im Neuenheimer Feld 280, 69120 Heidelberg, Germany. [6]Heidelberg Institute for Theoretical Studies (HITS), Schloss-Wolfsbrunnenweg 35, 69118 Heidelberg, Germany. [7]Department of Biomedicine, University of Bergen, Jonas Lies vei 91, 5009 Bergen, Norway.
*Present address: German Cancer Research Center, DKFZ, Im Neuenheimer Feld 280, 69120 Heidelberg, Germany. ‡Present address: European Molecular Biology Laboratory, Meyerhofstrasse 1, 69117 Heidelberg, Germany.
§These authors contributed equally to this work

¶Author for correspondence (freddy.frischknecht@med.uni-heidelberg.de)

C.A.M., 0000-0003-3412-2981; K.A.Q., 0000-0003-4134-3379; L.S., 0000-0002-0680-593X; F.F., 0000-0002-8332-6668

Received 2 October 2019; Accepted 6 January 2020

Journal of Cell Science (2021) 134, jcs233775. doi:10.1242/jcs.233775

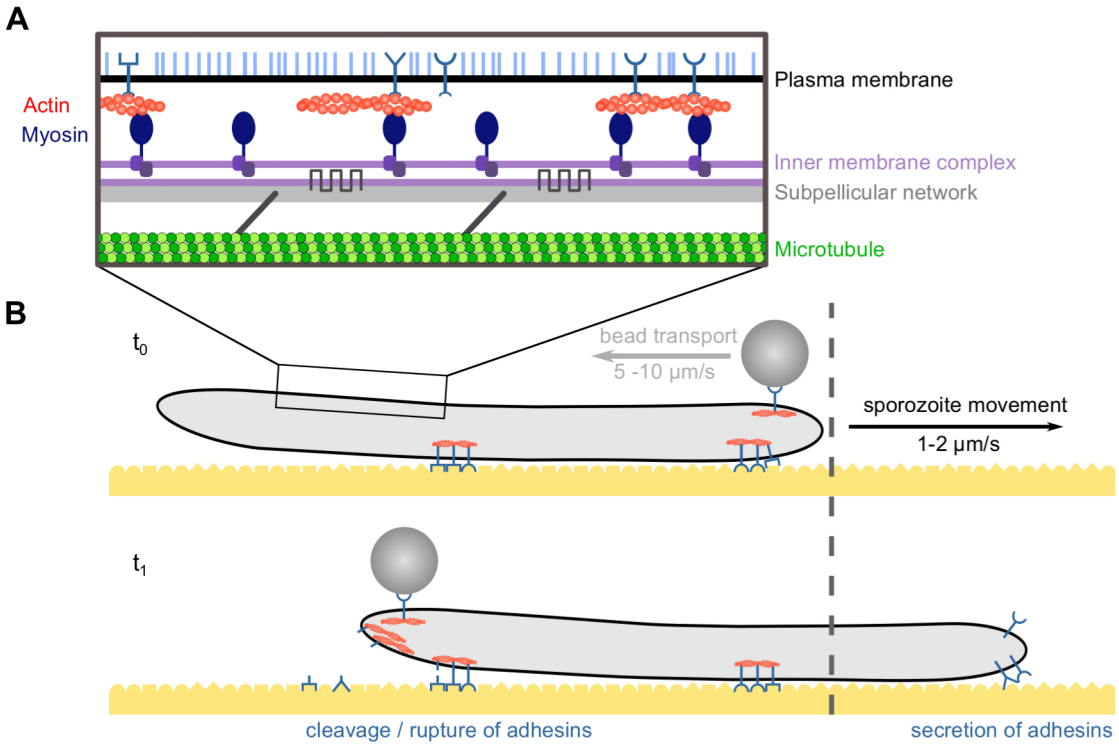

Fig. 1. Diagram illustrating gliding motility of *Plasmodium* sporozoites. (A) A model for the actin-myosin-based gliding machinery driving apicomplexan parasites including *Plasmodium* sporozoites. The plasma membrane mainly contains a glycosylphosphatidylinositol-anchored protein (the circumsporozoite protein in *Plasmodium* sporozoites) and additionally transmembrane proteins of which some are adhesins involved in linking actin filaments to the surface (bead or substrate or host cell membrane). Actin filaments are translocated backwards by myosin motors, which are in turn anchored through light chains and gliding-associated proteins to the inner membrane complex. Through proteins spanning the inner membrane, myosin is linked to the cytoskeletal sub-pellicular network underneath the inner membrane complex which, in turn, is linked to microtubules. (B) During sporozoite motility, particles engaging with the parasite surface are translocated rearwards at very high speed (5–10 µm/s), while parasites migrate at high speed (1–2 µm/s). During migration, parasite adhesins bind to the substrate and hence allow the force produced by myosin to be transmitted. Dynamic adhesion and de-adhesion cycles slow the parasite, and are likely modulated by the formation of assemblies made from adhesins and actin filaments. Adhesins disengage from the substrate and are cleaved by proteases towards the rear, where actin filaments accumulate. While the major traction forces are generated at the center of the parasites, stalling forces at the rear regulate migration.

filaments towards the rear end, where they might be depolymerized by coronin (Bane et al., 2016). Force is transmitted when membrane-spanning adhesins link these actin filaments to the substrate, while myosin pulls on the filaments (Heintzelman, 2015; Tardieux and Baum, 2016). This can lead to the retrograde flow of F-actin–adhesin complexes and the forward translocation of the sporozoite on a solid support. For *Plasmodium berghei* (*P. berghei*; *Pb*) sporozoites, the forces transmitted are of the order of 100 pN as measured by laser tweezers and traction force microscopy (Münter et al., 2009; Hegge et al., 2012; Quadt et al., 2016). This suggests that several dozens of myosins pull at a few filaments. These filaments might be oriented and organized by the actin filament-binding protein coronin and transmembrane adhesins of the thrombospondin-related anonymous protein (TRAP) family (Quadt et al., 2016; Bane et al., 2016). Actin filament turnover needs to be fast to keep the parasites moving at their high speed (Münter et al., 2009; Skillman et al., 2011; Douglas et al., 2018). Interfering with actin filament turnover by the addition of drugs or overexpression of profilin leads to non-motile sporozoites (Münter et al., 2009; Sato et al., 2016). Studies using amino acid substitutions in the actin-binding arm-motif of profilin have shown that sporozoite motility is affected by a lowered affinity of profilin to actin (Moreau et al., 2017). The acidic loop constitutes another divergent motif of apicomplexan profilins and is located on the opposing side of profilin from the actin-binding region (Fig. 2). Although the arm motif is conserved across Apicomplexa, the acidic loop is not conserved between species and can be very short. Here, we investigated whether the acidic loop can modulate actin binding or interfere with parasite motility by a set of different methods, including optical trapping, biochemistry, genetic engineering and molecular dynamic simulations. Currently, it is unclear which parameters of sporozoite motility are primarily affected by interfering with the motility machinery. In principle, these include retrograde flow, parasite speed, substrate adhesion, the percentage of motile sporozoites, persistence of motility and force generation. Probing a set of transgenic *P. berghei* parasites with laser tweezers revealed a contribution of the acidic loop to force production and retrograde flow, which emerge as the key factors at the origin of gliding motility.

RESULTS

Molecular dynamics simulations indicate possible effects of acidic loop mutations on the stability of the actin–profilin complex

Compared with human profilin, *Plasmodium* profilin contains several additional motifs, including a β-hairpin arm motif and an acidic loop (Fig. 2A). Comparison between different apicomplexan species shows that there is little difference in the arm motif (Moreau et al., 2017) while *T. gondii* profilin has only a very short acidic loop compared with the profilins in *Plasmodium* spp. (Fig. 2B,C). The regions bordering the acidic loop are highly conserved between *P. falciparum* and *P. berghei* profilin (100% over the 15 amino acid

Journal of Cell Science (2021) 134, jcs233775. doi:10.1242/jcs.233775

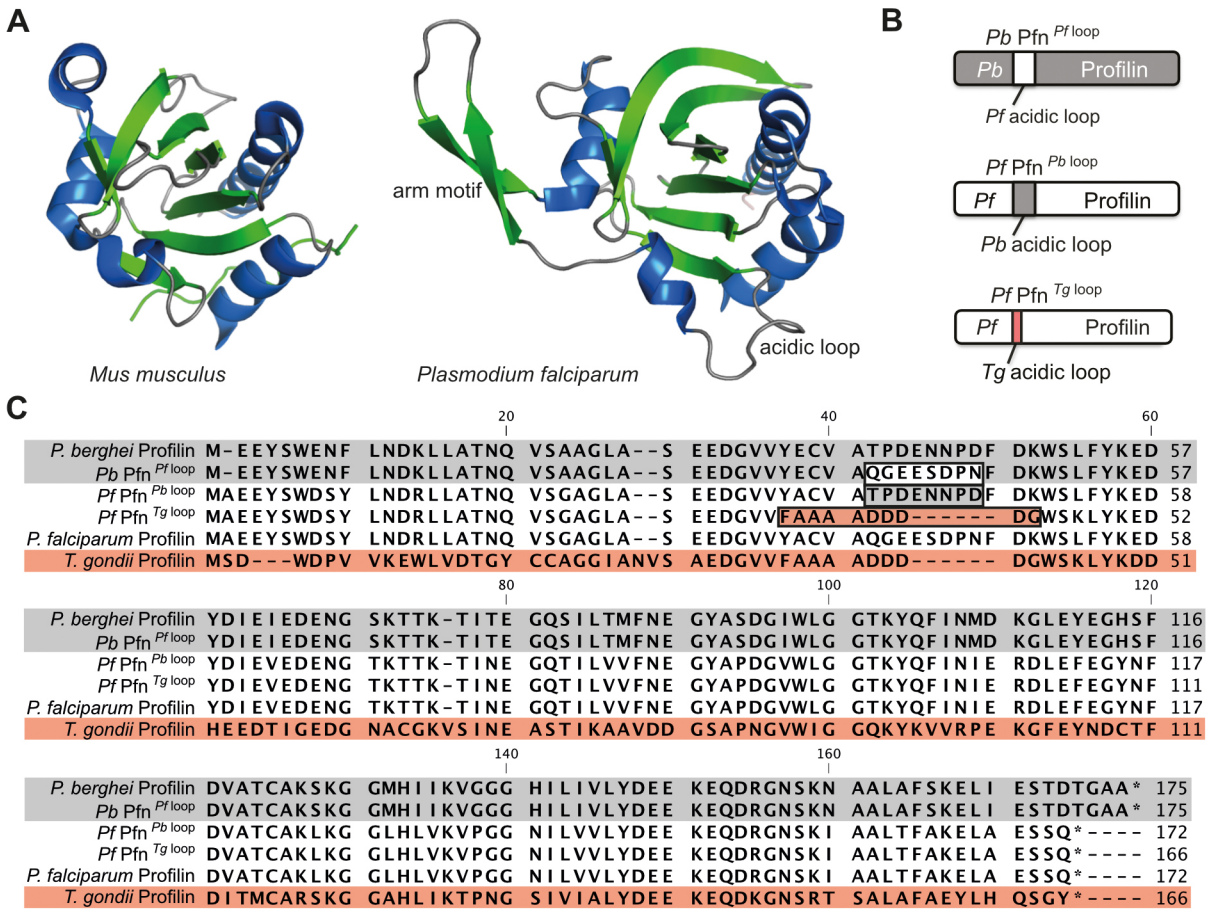

Fig. 2. Structural comparison between different profilins and mutant design. (A) Crystal structures of profilin from *Mus musculus* (PDB ID 2V8C, Kursula et al., 2008) and *P. falciparum* (PDB ID 2JKF, Kursula et al., 2008) show the Apicomplexa-specific additional domain. Green, β-strands; blue, α-helices. The arm motif and the acidic loop are labeled. (B) Schematic pictures of the different profilin chimeras generated with color coding as in panel C. Gray, *P. berghei*; white, *P. falciparum*; red, *T. gondii*. (C) Sequence alignment of *Plasmodium* and *T. gondii* profilins; the regions relevant for the chimeric mutants, as illustrated in B, are indicated. Gray background indicates the *P. berghei* profilin sequence and white the *P. falciparum* profilin sequence. Red background highlights the amino acid residues from *T. gondii* profilin transferred into the chimera. The boxes highlight the residues introduced in the three chimeras. The sequences were aligned using CLC Main Workbench software version 5.1 (CLC bio).

residues following the loop and only one A to E difference in the 15 amino acid residues preceding the loop). In contrast, six of the eight amino acid residues of the acidic loop are not conserved (Fig. 2B,C). The *T. gondii* profilin loop sequence is more divergent, consisting of just three aspartic acid residues. To investigate a potential role of the acidic loop in stabilizing the overall structure of profilin and in actin binding, we performed molecular dynamics simulations on a series of chimeric profilins similar to those described for the arm-motif mutations (Moreau et al., 2017). We designed the profilin acidic loop chimeras such that a *P. falciparum* profilin contained the loop of either *P. berghei* (*Pf* Pfn$^{Pb\,loop}$) or *T. gondii* (*Pf* Pfn$^{Tg\,loop}$) and also included a *P. berghei* profilin with a loop of *P. falciparum* (*Pb* Pfn$^{Pf\,loop}$) (Fig. 2B,C). In all simulations, we used *P. berghei* actin and therefore, from here onwards, 'actin' refers to *P. berghei* actin unless otherwise stated. The individual protein structures in the different complexes were stable in simulations as shown, for example, by the root-mean-square deviations (RMSDs) of the backbone atoms (Fig. S1). To study the effect of the different profilin chimeras on the actin–profilin interface, we performed a comparative analysis and calculated binding free energies. The calculated binding energies do not include translational, rotational and vibrational entropic contributions and therefore provide relative rather than absolute values of the binding free energies. The molecular dynamics simulations were performed for 500 ns and largely confirmed the differences in actin binding that we previously reported from 150 ns simulations for wild-type and mutant profilins with mutations from EDE to QNQ or AAA in the tip of the arm motif (Table S1, Movie 1).

Previously, we established that the acidic loop in the crystal structure of *Pf* Pfn (PDB ID 2JKF) is flexible, which may contribute to the physiological functions of Apicomplexa profilins (Kursula et al., 2008). Similar to the *Pf* Pfn crystal structure, we observed atomic fluctuations (B-factor) for the acidic loop residues in all of our molecular dynamics simulations except that for the *Pb* Actin–*Pb* Pfn$^{Pf\,loop}$ complex (Figs. S2 and S3, Movies 2 and 3, Tables S2 and S3). Low B-factor values in the loop region in the *Pb* Actin–*Pb* Pfn$^{Pf\,loop}$ complex apparently correlate with instability of the *Pb* Actin–*Pb* Pfn$^{Pf\,loop}$ complex as revealed by less favorable MM-GBSA and MM-PBSA binding energies throughout the simulations (Table S1, Fig. S4; see Materials and Methods). Interestingly, the *Pb* Actin–*Pf* Pfn$^{Tg\,loop}$ complex, with its shorter acidic loop, showed a tendency to larger variation in the MM-GBSA and MM-PBSA energies over the simulation than the complexes with wild-type *Pb* Pfn and the Pfn$^{Pb\,loop}$ (Fig. S4), suggesting that the loop length may influence the stability of the interactions at the actin–profilin interface.

Journal of Cell Science (2021) 134, jcs233775. doi:10.1242/jcs.233775

Biochemical assays reveal no differences in the actin binding of profilin loop mutants

The simulations indicated some differences between actin binding of *P. berghei* and *P. falciparum* profilin, which is in contrast to the similar force generating capacities of the *P. berghei* sporozoites expressing *P. falciparum* profilin (Moreau et al., 2017). The presence of other actin-binding proteins in the *in vivo* system may affect the dynamics of actin-mediated force.

To investigate these differences experimentally, we studied recombinant profilin chimeras in *in vitro* polymerization assays and by expressing them in parasites. We used overlap extension PCR to generate the different chimeric genes and expressed them in *E. coli* along with wild-type *P. falciparum* and *P. berghei* profilins, as described before (Moreau et al., 2017). We performed actin polymerization and co-sedimentation assays in the presence of the different purified profilins (Fig. S5). These assays showed that all chimeras had the same effect on actin polymerization as wild-type profilin (Fig. 3). Interestingly, the effect of *Plasmodium* profilin was more pronounced on *P. falciparum* actin polymerization than on pig skeletal muscle actin (α-actin) suggesting an important co-evolutionary constraint. Together with the molecular dynamics simulations, the *in vitro* polymerization assays suggest that actin polymerization requires minimal conserved interactions with the bound profilin, and these minimal interactions may remain conserved in different profilin acidic loop chimeras.

Reduction of sporozoite speed in profilin mutants

To test the chimeras *in vivo*, we generated a series of *P. berghei* strain ANKA parasite lines expressing the chimeras in place of the endogenous profilin (Fig. 4A–C). As the absence of introns does not influence life cycle progression or motility of parasites (Moreau et al., 2017), we introduced intron-free genes. As we have previously also shown that a C-terminal fluorescent protein tag could slow down parasites (Moreau et al., 2017), we further opted to exchange the genes without such a tag. After isolating clones from the different lines, we next investigated the progression of these through the life cycle (Table 1). We first compared the blood stage growth rates of the chimeric parasite lines to those of wild-type *P. berghei* and the previously reported *P. berghei* line expressing *P. falciparum* profilin. This showed that the parasites expressing the *P. berghei* profilin with the *P. falciparum* loop grew as fast as wild-type *P. berghei* (Moreau et al., 2017). Those lines expressing *P. falciparum* profilin and *P. falciparum* profilin with the *P. berghei* profilin loop grew somewhat faster but at comparable rates (Table 1). Intriguingly, expression of the *P. falciparum* chimera featuring the *T. gondii* loop slowed blood stage growth (Table 1), indicating that this chimeric profilin might not perform as efficiently *in vivo*. Infection of *Anopheles stephensi* mosquitoes, however, revealed similar infection rates and numbers of sporozoites. Infections of mice by mosquito bite showed a mild reduction in infectivity of the parasite lines expressing *P. falciparum* profilins containing *P. berghei* or *T. gondii* loops (Table 1). This could hint at a problem in their migration within the skin, their passing into or out of the blood stream or with liver stage growth. However, all mice develop a blood stage infection with the same time of onset, suggesting no defect in liver stage development. These assays comparing numbers of infected mosquitoes and colonizing parasites are comparatively insensitive due to their large biological variations. The most sensitive assay to dissect effects of subtle mutations affecting parasite motility is to investigate sporozoite motility on a glass surface (Bane et al., 2016; Moreau et al., 2017; Douglas et al., 2018). This assay has been used previously to show that *P. berghei* sporozoites expressing *P. falciparum* profilin migrate faster than wild-type *P. berghei* sporozoites, although fewer parasites are observed gliding (Moreau et al., 2017). Examination of the parasite lines expressing loop chimeras showed that sporozoites of all chimeras moved in the typical circular fashion of wild-type parasites (Fig. 4D). In all lines, about the same percentage of sporozoites were gliding, but curiously, those expressing *P. falciparum* profilin containing the loop of

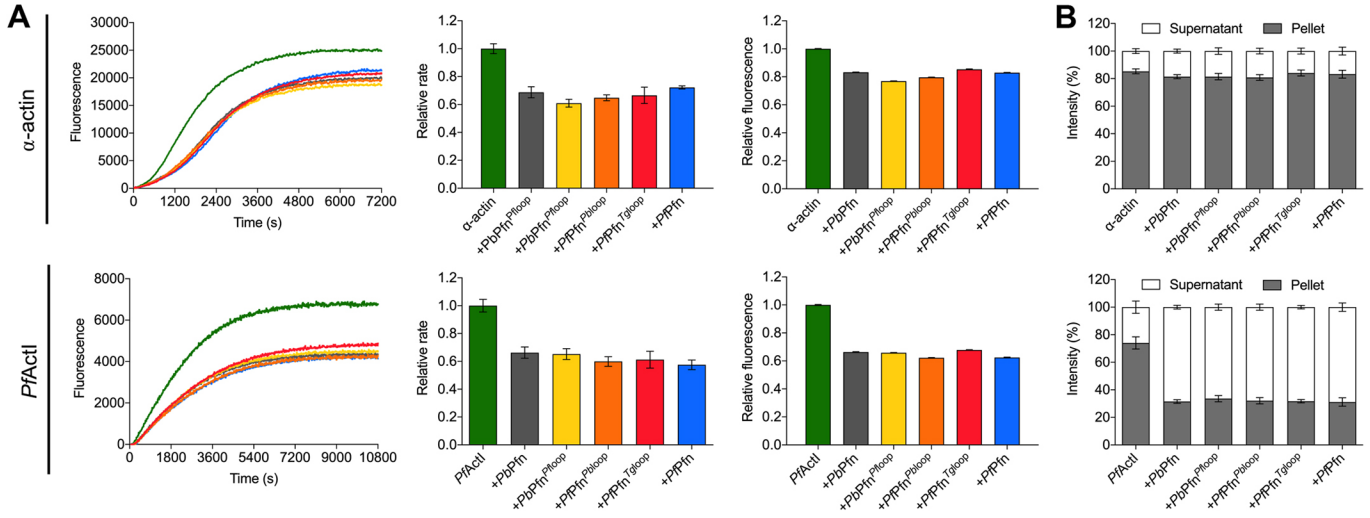

Fig. 3. The loop chimeras slow actin polymerization to a similar extent to that shown by wild-type profilin *in vitro*. (A) *In vitro* actin polymerization assays showing that all the profilin chimeras slow down actin polymerization to a similar extent to the wild-type *P. falciparum* and *P. berghei* profilins. 16 µM profilin was incubated with 4 µM *S. scrofa* (domestic pig) α-actin or *P. falciparum* actin 1, of which ∼5% and 2%, respectively, was labeled with pyrene. The polymerization kinetics were measured using a fluorescence plate reader with excitation and emission wavelengths of 365 and 407 nm, respectively. The initial polymerization rates and steady state levels (mean±s.d.; n=3), are plotted in the middle and right panels, respectively, for the timeframes of 1300–1800 s and 5500–6000 s for α-actin, and 500–1000 s and 9500–10,000 s for actin 1. (B) Co-sedimentation results showing that all chimeras sequester actin to a comparable extent to the wild-type *P. berghei* and *P. falciparum* profilins. Results are mean±s.d. for three independent experiments performed using the samples recovered from the polymerization assays. The original co-sedimentation gels are shown in Fig. S5.

Journal of Cell Science (2021) 134, jcs233775. doi:10.1242/jcs.233775

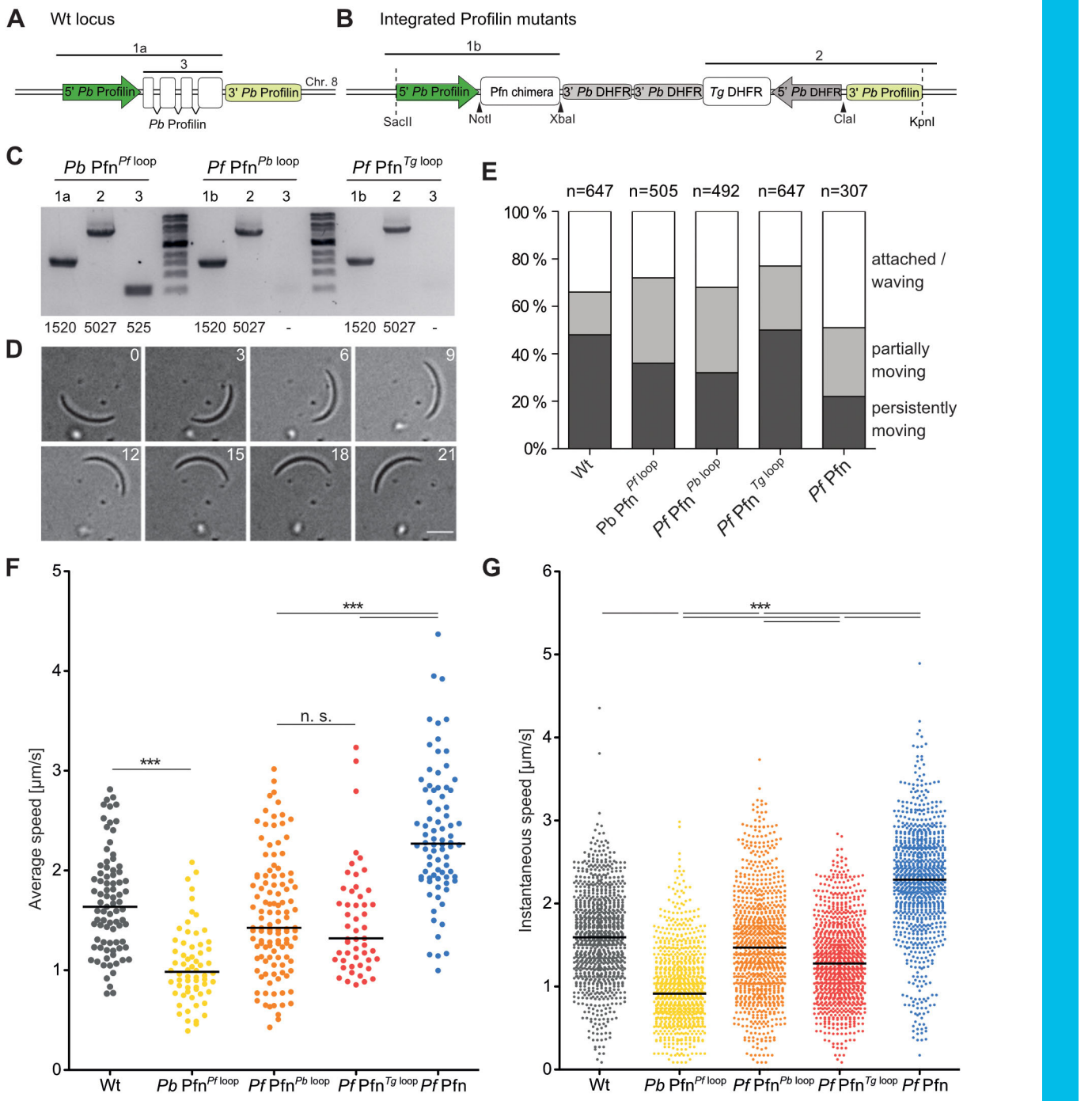

Fig. 4. Sporozoites expressing profilin chimeras move at slower speeds. (A–C) Generation of *P. berghei* lines expressing profilin chimeras. (A) Wild-type (Wt) locus showing the profilin gene with exons and introns located on chromosome 8. (B) Profilin locus after integration of the transfection plasmid. Note that the chimeric genes do not contain introns, so they can be distinguished from wild-type *Pb* Pfn. Amplicons used to investigate the resultant parasite lines in panel C are indicated with 1–3. Amplicon 3 was generated with *Pb* Pfn-specific primers. Restriction sites for cloning (arrowheads) and linearization (dotted lines) of the vector for transfection are indicated. (C) Agarose gel of PCR fragments obtained from the generated mutant lines. For wild-type integration, please see Moreau et al. (2017). (D) Time lapse image sequence showing the typical curved sporozoites migrating in a circular fashion. Numbers indicate time in seconds. Scale bar: 5 µm. (E) Distribution of movement phenotypes in the different parasite lines. White, sporozoites are attached and either do not move or wave; gray, sporozoites are partially moving; dark gray, sporozoites are persistently moving (for at least 150 s). (F) Average speeds of at least 40 sporozoites persistently moving for 150 to 300 s. The median speed of the population is indicated with a horizontal black line. ***P<0.01; n.s., not significant (Kruskal–Wallis test). (G) Instantaneous speeds from ten sporozoites with average speed closest to the median average speeds shown in F. Median instantaneous speeds of the populations are indicated with a horizontal black line. ***P<0.01 (Kruskal–Wallis test). Values for wild-type and *P. falciparum* profilin expressing lines were previously reported (Moreau et al., 2017).

T. gondii showed a higher percentage of persistently moving sporozoites than those just expressing the *P. falciparum* profilin (Fig. 4E). The quantification of their average and instantaneous speeds showed, however, that all sporozoites expressing chimeras were over 50% slower than their respective control parasite lines (Fig. 4F,G).

Journal of Cell Science

Journal of Cell Science (2021) 134, jcs233775. doi:10.1242/jcs.233775

Table 1. Comparative life cycle progression of parasite lines expressing profilin chimeras

Parasite line	Blood stage growth rate[a] (median)	Mosquito infection rate[b]	Oocysts/iMG[c] (mean)	MG spz/ mosquito (mean)	SG spz/ mosquito (mean)	Prepatency [d] (mean)	Parasitemia d6 [%] (mean)	C57BL/6 mice infected
Pb wild type	8.9	50	105	39,000	9400	3.75	2.3±0.4	4
Pb Pfn$^{Pf\ loop}$	8.4	33	90	23,000	5000	3.75	1.9±0.5	4
Pf Pfn$^{Pb\ loop}$	10.8	25	75	19,000	4600	4.5	0.8±0.3	4
Pf Pfn$^{Tg\ loop}$	7.7	25	100	22,000	3800	4.83	0.7±0.1	6
Pf Pfn	10.5	33	75	36,000	4300	4	1.7±0.8	4

[a]24 h *in vivo* multiplication rate. [b]Percentage infected of all mosquitoes in a cage used for a blood feed. [c]Mean number of oocysts in midguts showing at least one oocyst. More than 50 infected midguts were counted for each parasite line.
MG, midgut; SG, salivary gland; Prepatency, time to observation of blood stage parasites; Parasitemia, percentage of parasitized red blood cells. Note that the values for wild-type and *P. falciparum* profilin-expressing lines were previously reported (Moreau et al., 2017).

Lowered forces and increased retrograde flow in profilin mutants

A slower sporozoite speed could be due to multiple factors such as elongated, shortened or misaligned actin filaments (Münter et al., 2009; Quadt et al., 2016; Hegge et al., 2012; Bane et al., 2016). This might cause a shift in the dynamics of adhesion formation and a diminished capacity to generate force onto the substratum (Münter et al., 2009; Quadt et al., 2016). Diminished forces were shown to correlate with faster retrograde flow on the sporozoite surface in two previous studies (Moreau et al., 2017; Quadt et al., 2016). Analysis of mutations in the arm motif of *P. falciparum* profilin have shown that sporozoites that move as well as wild-type controls can show differences in their capacity to generate force and in the speed of retrograde flow as measured by optical tweezers (Moreau et al., 2017). As the sporozoites expressing chimeras moved at diminished speed, we next probed whether their capacity to generate forces and retrograde flow differed from the respective control sporozoites. Laser tweezers can deliver polystyrene beads onto the surface of the sporozoite, which allows two types of experiments. In the first type, the bead is bound by the sporozoite, pulled out of the weak laser trap and actively transported towards the rear end of the parasite due to the retrograde flow of membrane proteins likely coupled to the actin-myosin motor (Fig. 5A,B). In the second type, the bead is bound by the sporozoite, but the trap is kept at a high counterforce such that the parasite struggles to pull the bead out of the trap (Fig. 5B). The number of sporozoites that are capable of pulling beads out of a trap at a constant force was quantified and used to compare different parasite lines as in our previous studies (Moreau et al., 2017; Quadt et al., 2016).

We first tracked the speed of the bead transport along the sporozoite (Fig. 5C) then determined peak speeds of retrograde flow (Fig. 5D), which showed that *P. berghei* (*Pb*) sporozoites expressing chimeric profilins could transport the beads faster than control sporozoites (Fig. 5E). As reported previously, wild-type parasites transported beads with an average peak speed of 6.7 µm/s (Moreau et al., 2017). Similarly, sporozoites expressing *P. falciparum* (*Pf*) profilin (Pfn) transported beads at an average of 6.1 µm/s (Fig. 5E). In contrast, sporozoites expressing the chimeras transported beads ∼30 to 40% faster (9.4 µm/s, *Pb* Pfn$^{Pf\text{loop}}$; 10.4 µm/s, *Pf* Pfn$^{Pb\text{loop}}$ and 10.3 µm/s, *Pf* Pfn $^{Tg\text{loop}}$).

We next measured the forces the sporozoites expressing chimeric profilins could generate. At 70 pN of optical force, 74% of wild type and 71% of sporozoites expressing *Pf* Pfn could pull a bead from a trap (Moreau et al., 2017, Fig. 5F). Sporozoites expressing the Pfn chimeras were only able to pull 31% (*Pb* Pfn$^{Pf\text{loop}}$), 37% (*Pf* Pfn$^{Pb\text{loop}}$) or 51% (*Pf* Pfn$^{Tg\text{loop}}$) of beads out of a trap of the same strength (Fig. 5F). A similar trend was seen at 130 pN, where wild-type and *Pf* Pfn expressing sporozoites could still pull 38% and 32% of beads out of the trap. At this force, the chimera-expressing sporozoites could only pull 13%, 16% and 24% out of the trap, respectively (Fig. 5F). These data support what we have observed for other mutants: retrograde flow speed peaks correlate inversely with force capacity. Interestingly, the other parameters – such as gliding speed, percentage of motile parasites and actin binding – from this and our previous studies (Moreau et al., 2017; Quadt et al., 2016) show less or no such correlation (Table 2).

DISCUSSION

Plasmodium profilin is a key regulator of actin dynamics and is likely essential for efficient blood stage growth and infectivity (Jacot et al., 2016; Kursula et al., 2008). Subtle mutations in the arm motif showed that this motif is important for efficient sequestration of actin monomers *in vitro* as well as for ookinete and sporozoite motility (Moreau et al., 2017). The presence of a highly divergent acidic loop in the apicomplexan-specific domain of profilin suggested to us that it has a possible role in profilin function. This loop could either bind to additional factors or play a role in the flexibility of the profilin monomer with an allosteric effect on actin binding. To probe the function of this loop, we generated a series of chimeric proteins that contained the acidic loop of *P. berghei* and *T. gondii* swapped into the *P. falciparum* profilin, as well as one with the *P. falciparum* loop in *P. berghei* profilin (Fig. 2B,C). Molecular dynamics simulations suggested that one of the chimeras (*P. berghei* profilin with the *P. falciparum* profilin acidic loop) might have a weakened actin binding capacity (Table S1). To investigate these results experimentally, we combined our recently established molecular genetics and biochemical workflow to investigate profilin function *in vitro* and *in vivo* (Moreau et al., 2017). Biochemical investigations showed that purified *P. berghei* profilin, despite sharing only 76% identity with *P. falciparum* profilin (Kursula et al., 2008), sequestered actin monomers as efficiently (Fig. 3). This was not surprising, as the force generation capacity of *P. berghei* sporozoites expressing *P. falciparum* profilin was the same as that of wild-type *P. berghei* (Moreau et al., 2017). Notably, profilin interacted 'better' with actin from *P. falciparum* than with mammalian muscle actin, suggesting a co-evolutionary adaptation of the two proteins. The fact that all the chimeras showed a full sequestration capacity further suggests that the actin–profilin interface is hardly altered between the profilins. It also suggests that the acidic loop plays no role in actin binding *in vitro*. As all chimeras could replace the natural profilin in *P. berghei*, the acidic loop also does not seem to play an essential role *in vivo*, although expression of *Pf* Pfn containing the *Tg* loop led to slower blood stage growth. None of the parasite lines expressing the different profilins showed a phenotypic difference until transmission from the mosquito back to the mouse, where again the *Pf* Pfn$^{Tg\text{loop}}$ parasite line showed the lowest infectivity, with about half a day delay in blood stage

Journal of Cell Science (2021) 134, jcs233775. doi:10.1242/jcs.233775

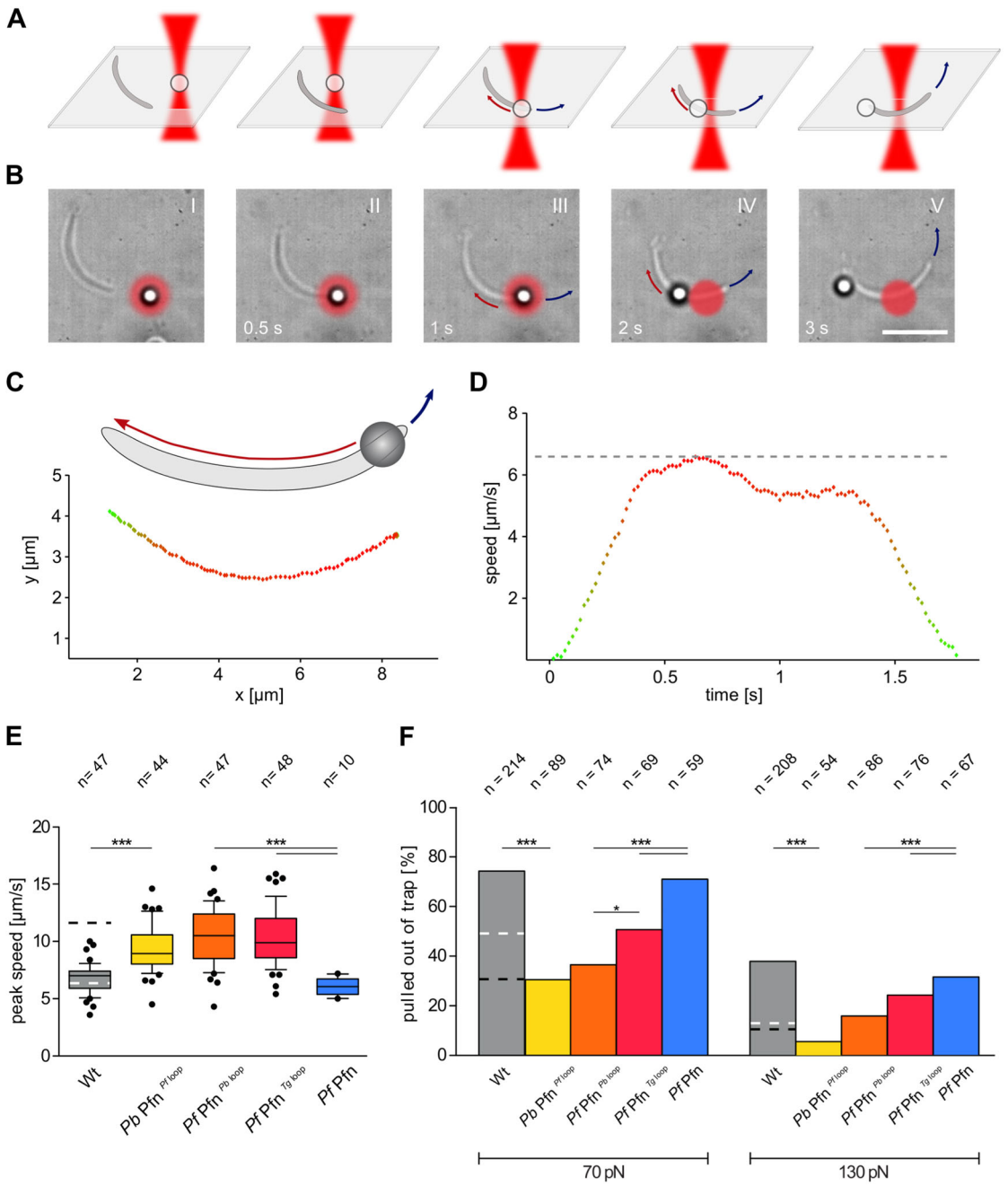

Fig. 5. Sporozoites expressing profilin chimeras produce less force but faster retrograde flow. (A,B) Image series of optical tweezers experiments. (A) Schematic sequence: a bead caught in the focus of the laser trap (shown in red) (I) is moved towards the sporozoite (II) and lowered down onto the front end of a sporozoite that moves on a solid support (III). After contact (bead and sporozoite both in focus), the sporozoite pulls the bead out of the trap center (IV) and actively transports the bead to the rear of the cell (V). (B) Corresponding time lapse to A showing the experimental sequence for retrograde flow of a bead on a sporozoite. Arabic numbers (bottom left) indicate time in seconds. Scale bar: 10 µm. Red arrow, bead transport direction; blue arrow, sporozoite gliding direction. (C) Diagram of bead transport and trajectory of tracked bead positions during transport. A bead positioned onto the front end of a counterclockwise moving sporozoite is subsequently transported along the cell. Note that the sporozoite is moving to the right and the bead is moving to the left. Red arrow, bead transport direction; blue arrow, sporozoite gliding direction. Color code of trajectory, fast speed is shown as red dots, and slow speed in green [i.e. at the start of movement (acceleration not visible) and during deceleration]. (D) Speed plot of the transported bead from C with determined peak speed at 6.6 µm/s indicated by dashed line in light gray. Fast speed is shown in red, and slow speed (i.e. start of movement and deceleration) in green. (E) The peak retrograde flow speed on sporozoites expressing profilin chimeras is faster than in control parasites. The boxes contain 50% of the values, 15% are displayed on each whisker and another 10% (outliers) on each side are depicted as dots. Numbers above indicate the total number of sporozoites investigated. ***P<0.001 (one-way ANOVA). Median values for wild-type and *P. falciparum* profilin expressing lines were previously reported (Moreau et al., 2017). White dashed line indicates median values of wild-type sporozoites treated with cytochalasin D. Black dashed line indicates median values of wild-type sporozoites treated with jasplakinolide. Both values were previously reported in Quadt et al. (2016). (F) Cumulative percentage of sporozoites that could pull a bead out of a trap at the indicated optical force of 70 or 130 pN. Numbers above indicate the total number of sporozoites investigated. *P<0.05, ***P<0.001 (Fisher's Exact test). Median values for wild-type and *P. falciparum* profilin-expressing lines were previously reported (Moreau et al., 2017). White dashed lines indicate median values of wild-type sporozoites treated with cytochalasin D. Black dashed lines indicate median values of wild-type sporozoites treated with jasplakinolide. Both values were previously reported in Quadt et al. (2016).

Journal of Cell Science (2021) 134, jcs233775. doi:10.1242/jcs.233775

patency (i.e. the time it takes from injecting sporozoites to seeing first blood stage parasites) (Table 1). However, these subtle differences need to be interpreted carefully as slightly different numbers of injected sporozoites can be the reason for such a small delay. To test whether such a difference is significant would require the infection of a large number of mice (see e.g. Bane et al., 2016), which we feel is not justified by the goal of the study. Importantly, even the mutations in the actin-binding arm motif did not cause a measurable delay in mouse infectivity (Moreau et al., 2017). However, clear effects on *Plasmodium* sporozoite motility could be distinguished between the mutants.

Previously, we found that expressing *P. falciparum* profilin (*Pf* Pfn) speeds up sporozoites that migrate on a flat surface (Moreau et al., 2017). The sporozoites expressing *Pf* Pfn with either the *Pb* or the *Tg* loop were considerably slower than *Pf* Pfn sporozoites (Fig. 4F,G) and moved in greater numbers (Fig. 4E). Similarly, sporozoites expressing *Pb* Pfn containing the *Pf* loop were also slower than wild-type *P. berghei* sporozoites (Fig. 4F,G). This clear trend across all parasite lines suggests that the loop determines part of the function of profilin in sporozoite motility. Intriguingly, this slowing of motility could not be linked to a difference in actin binding *in vitro* suggesting that the loop might play a role *in vivo* by interacting with other proteins or lipids that are missing in the *in vitro* assays. For example, the actin-nucleating *Plasmodium* formin, localized at the tip of the sporozoite, could interact differentially with the different profilins (Ignatev et al., 2012; Douglas et al., 2018). To identify other partners of profilin, pulldowns with GFP-tagged profilin or proximity labeling (Kehrer et al., 2016) could be employed.

We have previously shown that beads trapped by a focused laser beam can be used to measure the retrograde flow on the sporozoite surface and the force that sporozoites are able to generate (Quadt et al., 2016). We applied this approach to measure the forces generated by two different parasite lines that were mutated in the key actin-interacting region of the profilin arm motif. These two parasite lines featured the sequences QNQ or AAA instead of the natural acidic EDE at the tip of the arm motif. Interestingly, those featuring the QNQ motif could still move as well on glass as the control parasites, while those with the AAA motif largely failed to move persistently. However, laser tweezer measurements revealed that both lines showed an increased retrograde flow rate but produced significantly less force (Moreau et al., 2017). These observations, together with data suggesting that coronin and TLP might orient actin filaments for efficient motility (Quadt et al., 2016; Bane et al., 2016), suggested to us that a critical number of filaments, as well as unknown factors, govern the transition of force generation to motility (Moreau et al., 2017). We envisage that a macromolecular complex containing adhesins and actin filaments is assembled at the tip of the parasite, and that a perturbation of this can have different non-linear effects on force, retrograde flow and the capacity to glide. All sporozoites expressing chimeric profilins showed an increased retrograde flow and a decreased force, just like those sporozoites lacking the TRAP family adhesin TLP (Quadt et al., 2016) or the profilin arm motif mutants (Moreau et al., 2017). It is interesting to note that the *Pf* Pfn chimera expressing the *Tg* loop showed the highest capacity to generate force (Fig. 5F), although this should be interpreted carefully. Indeed, these sporozoites migrated as well as those expressing the *Pb* loop in *Pf* Pfn (Fig. 4E). Modification of the profilin loop thus might lead to subtle changes in the motility of sporozoites that are comparable to those observed with parasites lacking the TRAP-like protein TLP (Hegge et al., 2010; Quadt et al., 2016; Hellmann et al., 2011). Profilin is currently the only protein that has been modified to yield either faster (when profilin from *P. falciparum* is expressed in *P. berghei*) or slower sporozoites (when profilin from *P. falciparum* carrying the arm motif mutation AAA is expressed in *P. berghei*; Fig. 6). This indicates a dual effect on actin dynamics similar to those mediated by cytochalasin D (CytoD) or jasplakinolide (jas) (Quadt et al., 2016) (Table 2). Intriguingly, the most consistently observed effect during genetic or chemical perturbation of gliding sporozoites is the inverse relationship between retrograde flow and force (Table 2). This suggests to us that the trapping of adhesins that are transported to the rear into macromolecular assemblies (and hence the slowing down of adhesins) is essential for the generation of stronger force. This in turn can affect the speed of sporozoite motility, while actin binding appears to primarily affect the percentage of motile sporozoites (i.e. robustness of gliding).

Clearly, more work is needed to put these data into a holistic molecular model of gliding motility that also depends on the formation and turnover of distinct adhesion sites (Münter et al., 2009), a process that cannot be directly investigated with optical traps during sporozoite gliding (Hegge et al., 2012). Ultimately, the visualization or biochemical reconstitution of the macromolecular complexes and actin nucleation by formins at the tip of the sporozoite will be essential for a more complete understanding of parasite migration.

Conclusions

Our data show that the actin-binding protein profilin can be mutated in a way that does not affect actin polymerization *in vitro* but still has a measurable impact on gliding motility of *Plasmodium* sporozoites. All three mutants investigated showed robust but slower motility and

Table 2. Correlation of parameters describing sporozoite gliding motility

	Actin binding	Motile sporozoites	Sporozoite speed	Retrograde flow	Force generation
WT	+++	+++	++	++	+++
WT – CytoD	n.d.	++	+	++	+
WT – Jas	n.d.	++	+++	+++	+
tlp(-)	n.d.	+++	++	+++	+
Pf Pfn	+++	++	+++	++	+++
Pf Pfn QNQ	++	++	+++	+++	+
Pf Pfn AAA	+	+	+	+++	+
Pb Pfn^{Pfloop}	+++	+++	+	+++	+
Pf Pfn^{Pbloop}	+++	+++	++	+++	+
Pf Pfn^{Tgloop}	+++	+++	++	+++	++

+, low; ++, medium; +++, high; n.d., not determined.

Key gliding motility parameters determined in this and other (Moreau et al., 2017; Quadt et al., 2016) studies show the high level (7/8) of inverse correlation between retrograde flow and force generation upon a perturbation from the controls. Other parameters correlate much less with each other. Only treatment with cytochalasin D yields no difference in retrograde flow while force drops, suggesting that not all membrane flow is coupled to actin filaments as suggested in *T. gondii* (Gras et al., 2019).

Journal of Cell Science (2021) 134, jcs233775. doi:10.1242/jcs.233775

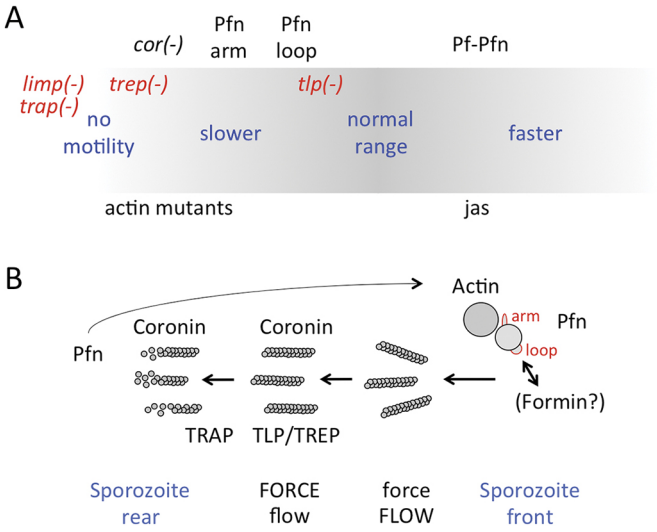

Fig. 6. Diagrams contextualizing the data. (A) The effects of different modified or deleted parasite proteins, and of the addition of small concentrations of the actin-stabilizing drug jasplakinolide (jas) on *P. berghei* sporozoite motility are indicated. Among secreted proteins (red), the deletions of *trap* and *limp* produce the most severe effects, generating only very few sporozoites capable of invading salivary glands (Sultan et al., 1997; Santos et al., 2017); *cor(-)*, deletion of coronin (Bane et al., 2016). Pfn arm depicts the EDE to AAA mutation at the tip of the profilin arm motif, and Pf-Pfn the expression of *P. falciparum* profilin in place of *P. berghei* profilin (Moreau et al., 2017). The Pfn loop and *tlp(-)* (Quadt et al., 2016) mutants show motility close to the 'normal range' of wild-type *P. berghei* sporozoites. Note that more proteins that modulate sporozoite motility have been investigated than are depicted including ICP (Lehmann et al., 2014), CelTOS (Steel et al., 2018), α-tubulin (Spreng et al., 2019) and IMC-associated proteins (Khater et al., 2004; Volkmann et al., 2012). Profilin is the only protein that can be mutated such that sporozoites move either faster or slower. (B) *Plasmodium* profilin binds and sequesters actin with the help of its arm domain. The actin-filament-nucleating formin is localized at the tip of sporozoites (Douglas et al., 2018). Profilin might interact with formin or another partner using the acidic loop domain. Actin filaments formed are organized by coronin (Bane et al., 2016) and the TRAP family adhesins (Hegge et al., 2010; Quadt et al., 2016) leading to optimal force generation by myosins (not shown). At the rear, coronin might contribute to actin depolymerization (Bane et al., 2016).

lower force production capacity than the respective control parasite lines while being able to generate faster retrograde flow. This suggests that the interplay between the retrograde flow of adhesins and force generation is regulated in a complex manner and is the key for understanding gliding motility in apicomplexan parasites.

MATERIALS AND METHODS

Molecular dynamics simulations

For preparation of structures, the crystal structures of *P. falciparum* actin 1 (PDB ID 4CBU, 0.13 nm resolution; Vahokoski et al., 2014) and *P. falciparum* profilin (PDB ID 2JKF, 0.231 nm resolution; Kursula et al., 2008) were retrieved from the RCSB-PDB database (Berman et al., 2000). These structures were aligned to the crystal structure of rabbit α-skeletal muscle actin co-crystallized with human profilin (PDB ID 2PAV, 0.231 nm resolution; Ferron et al., 2007). The thus obtained *P. falciparum* actin–profilin complex was prepared for simulations using the Protein Preparation Wizard module of Schrodinger (version 2016r1). In brief, the complex was pre-processed to assign bond orders, to add missing hydrogen atoms and to add missing side chains. Co-crystallized waters were kept in the complex structure. PROPKA (Dolinsky et al., 2007) was used to predict the protonation states at pH 7.0 of the titratable residues. Missing residues were modeled using the Prime module in the Schrodinger software. Note that the *P. falciparum* and *P. berghei* actin only differ in three amino acid residues (E3, D5 and V11 of *P. falciparum* actin are D, E and I, respectively, in *P. berghei* actin), which are distant from the conventional actin–profilin interface.

To model *P. berghei* profilin (*Pb* Pfn), the *P. berghei* profilin sequence was retrieved from the PlasmoDB database (Aurrecoechea et al., 2009) and modeled using PRIME software using the *P. falciparum* profilin (*Pf* Pfn) structure (75.9% identical to *P. berghei* profilin) as the template structure. Next, we used these *P. falciparum* profilin and (modeled) *P. berghei* profilin structures as templates to model the three chimeric mutants (*Pb* Pfn$^{Pf\text{loop}}$ using *Pb* Pfn as template, *Pf*Pfn$^{Pb\text{loop}}$ and *Pf*Pfn$^{Tg\text{loop}}$ using *Pf* Pfn as template) by changing the acidic loop residues shown in Fig. 2C.

For molecular dynamics simulations, the modeled protein complexes were prepared for all-atom molecular dynamics simulations using the tleap program in the AMBER molecular dynamics package version 14 (http://ambermd.org/; Cerutti et al., 2014). ATP parameters were taken from the AMBER parameter database (http://research.bmh.manchester.ac.uk/bryce/amber; Meagher et al., 2003). GAFF (Wang et al., 2004) and ff14SB (Cerutti et al., 2014) parameters were assigned to the ligand and protein, respectively. Non-bonded interactions were cut off at 0.8 nm and the particle mesh Ewald method was applied. The systems were solvated using the TIP3P water model (Price and Brooks, 2004) in a truncated octahedral box. Na^+ and Cl^- ions were added to obtain an ionic strength of 50 mM, and the systems were neutralized using Na^+ counter-ions. A two-step minimization was performed on each system as follows: 1000 steps of minimization while keeping restraints (force constant 100 kcal/mol Å^2) on the solute (protein and ligands; first 500 steps of steepest descent, next 500 steps of conjugate gradient) followed by all-atom minimization (first 1500 steps of steepest descent, next 1500 steps of conjugate gradient). The minimized systems were gradually heated (0 to 298 K in 80 ps) using the canonical ensemble (NVT) at each temperature point. In the next step, the pre-heated systems were equilibrated in an isothermal–isobaric ensemble (NPT) at 298 K. Berendsen temperature coupling and a constant pressure of 1 atm with isotropic molecule-based scaling was used in the equilibration. The SHAKE algorithm (Ryckaert et al., 1977) was applied to constrain all covalent bonds containing hydrogen atoms and a time step of 2 fs was used. All systems were simulated with periodic boundary conditions in the NPT ensemble for 500 ns. The analysis of the molecular dynamics trajectories was carried out with the CPPTRAJ module of AMBER 14. VMD (version 1.9.2), Chimera (version 1.10) and Pymol (version 1.8.2.3) were used for visualization.

For binding free energy calculations, the molecular mechanics energies combined with the Poisson Boltzmann or generalized Born and surface area continuum solvation (MM-PBSA and MM-GBSA) energies were used to estimate the actin–profilin binding free energy. The snapshots were retrieved at an interval of 1 ns from the last 200 ns of the molecular dynamics trajectories (between 300 and 500 ns). Because the current study involves the comparison of similar systems, we did not explicitly calculate entropic contributions to the binding free energy, and we assumed they were similar in all cases. Therefore, the calculated energies do not correspond to the absolute free energies but can be used to compare similar systems.

Recombinant protein production and biochemical work

Profilin chimeras were generated using overlap extension PCR and cloned into pETM-11 (Moreau et al., 2017) using *Nco*I and *Xho*I restriction sites. Wild-type *Pf* (Ignatev et al., 2012) and *Pb* as well as chimera Pfns were expressed in *E. coli* BL21(DE3) cells and purified using standard protocols. More precisely, cells were lyzed by sonication in lysis buffer (10 mM Tris-HCl pH 7.5, 300 mM NaCl and 5% glycerol), and clarified lysates were incubated with HisPur Ni-NTA resin (Thermo Scientific). Resins were washed with lysis buffer supplemented with 0, 10 and 25 mM imidazole, and finally proteins were eluted with 300 mM imidazole in the lysis buffer. Proteins were dialyzed against 10 mM Tris-HCl pH 7.5, 50 mM NaCl and 2% glycerol. Purification tags were cleaved either with TEV during dialysis (in the case of *Pb* and chimera Pfns) or thrombin after dialysis (in the case of *Pf* Pfn). After tag cleavage, proteins were again passed through HisPur resin and gel filtered using HiLoad Superdex S75 preparative grade 16/60 column (GE Healthcare). Peak fractions were checked for purity by SDS-PAGE, concentrated and stored on ice. Domestic pig (*Sus scrofa*) skeletal muscle α-actin was purified as described previously (Ignatev et al., 2012; Pardee and Spudich, 1982). *Pf* actin 1 was expressed in *Spodoptera frugiperda Sf*21

cells (Invitrogen) as described previously (Ignatev et al., 2012) with minor changes in the protocol. Firstly, 7 µl of high-titer virus was used to infect 10^6 cells, and secondly, the cells were harvested 4 days after infection and used immediately for protein purification as described in Moreau et al. (2017).

The effects of *Pb*, *Pf* and chimera profilins on α-actin and *Pf* actin 1 polymerization kinetics were studied with fluorescence spectroscopy using ∼5% and 2% pyrene-labeled α-actin and *Pf* actin 1, respectively, in 10 mM HEPES pH 7.5, 0.2 mM $CaCl_2$, 0.5 mM ATP, 0.5 mM TCEP. Polymerization of 4 µM actin alone and in the presence of 16 µM *Pf* Pfn, *Pb* Pfn, *Pb* $Pfn^{Pf loop}$, *Pf* $Pfn^{Pb loop}$ or *Pf* $Pfn^{Tg loop}$ (in triplicates) was induced by adding polymerizing buffer to final concentrations of 50 mM KCl, 4 mM $MgCl_2$ and 1 mM EGTA. Polymerization was followed for 2 and 3 h in the case of α-actin and *Pf* actin 1, respectively, by measuring the increase in fluorescence signal upon incorporation of pyrene-labeled actin into growing filaments using a Tecan M1000 Pro plate reader at 25°C with excitation and emission wavelengths of 365 and 407 nm, respectively. The assays were repeated twice.

All polymerization curves were set to start from zero fluorescence intensity, and the initial polymerization rates were determined as the slopes of linear fits to the polymerization data between 1300 and 1800 s for α-actin and between 500 and 1000 s for *Pf* actin 1. The relative initial polymerization rates were obtained by dividing the initial polymerization rate values by the initial polymerization rate of *Pf* actin 1 alone. Plateau levels of the polymerization curves were determined as average values from the range of 5500–6000 s and 9500–10,000 s for α-actin and actin 1, respectively.

For co-sedimentation experiments, 100 µl of each polymerization sample (still as triplicates) were recovered from the 96-well plate. Samples were centrifuged for 1 h at 20°C using speeds of 48,000 and 100,000 rpm for α-actin and *Pf* actin 1, respectively, using a TLA-100 rotor (Beckman Coulter), and the resulting supernatants and pellets were separated. The supernatants were mixed with 25 µl of 5× SDS-PAGE sample buffer (250 mM Tris-HCl pH 6.8, 10% SDS, 50% glycerol, 0.02% Bromophenol Blue and 1.43 M β-mercaptoethanol), and the pellets were resuspended in 125 µl of 10 mM HEPES pH 7.5, 0.2 mM $CaCl_2$, 0.5 mM ATP, 0.5 mM TCEP supplemented with 1× SDS-PAGE sample buffer. Samples were incubated 5 min at 95°C, and then 12.5 µl of each sample was analyzed on 4–20% SDS-PAGE gels. The protein bands were visualized with PageBlue stain (Thermo Scientific). Gels were imaged using the ChemiDoc XR S+ system and protein band intensities were determined with the Image Lab 3.0 software (both from Bio-Rad). For each supernatant and pellet pair, the total intensity of *Pf* actin 1 was set to 100% and relative amounts of actin 1 in supernatants and pellets were presented as percentages of that. The assays were repeated twice.

Molecular cloning and parasite generation

Vectors used for *in vivo* work are based on the b3D+ vector (Silvie et al., 2008). Integration primers (Table S4) correspond to fragment numbers in Fig. 4. We modified the vector for homologous recombination in the profilin (PBANKA_0833000) locus on chromosome 8 as follows. The *P. berghei* profilin 5′ upstream region (871 bp) was amplified from *P. berghei* ANKA WT genomic DNA using primer combination 5 (Table S4) and subsequently inserted into b3D+ via *Sac*II and *Not*I digestion and ligation. The profilin 3′ downstream region (805 bp) was amplified with primer combination 6 and inserted using *Cla*I and *Kpn*I.

Wild-type *P. berghei* profilin was amplified with primer combination 3 and cloned with *Not*I and *Xba*I. Wild-type *P. falciparum* profilin was amplified with primer combination 4 and cloned into b3D+ using *Not*I and *Xba*I. Profilin chimeras were generated by overlap extension PCR where the respective loop regions were encoded by the interior primers generating two fragments (A and B). The loop regions present in both fragments were then used to anneal and fuse the fragments together. The *Pb* Pfn loop was encoded in primers 7a and 7b, the *Pf* Pfn loop in primers 8a and 8b and the *Tg* Pfn loop by primers 9a and 9b (Table S4).

Parasite transfection and sporozoite generation

All transfections and generation of clonal parasite lines were performed as previously described (Janse et al., 2006). All vectors were linearized with *Sac*II and *Kpn*I prior to transfection. A PCR to probe correct integration was performed after limiting dilution cloning (Fig. 4). *Anopheles stephensi* mosquitoes were infected with clonal lines as follows. Infected mouse blood was injected intraperitoneally into a naïve NMRI mouse. At a parasitemia of >1%, the blood was harvested and 10–20 million parasites were injected intraperitoneally into two or three naïve mice. After 3–4 days, these mice were anesthetized and positioned on top of a mosquito cage to allow mosquitoes to feed. Mosquitoes were analyzed for oocyst numbers on day 12 and for midgut and salivary gland sporozoites on days 17–23.

Assessment of parasite function across the life cycle

We determined parasite growth rates by injecting 100 or 5000 infected red blood cells into each of four C57BL/6 mice. Parasitemia was monitored daily starting on day 3. We calculated parasite growth rate as described previously (Spaccapelo et al., 2010; Klug et al., 2016). Oocyst numbers were determined by extracting midguts of infected mosquitoes on day 12 after infection. Midguts were stained for 20 min using 0.1% mercurochrome solution (Moll et al., 2008). Stained oocysts were counted using a 10× objective in at least 50 infected midguts.

Imaging was performed using an inverted Axiovert 200M microscope (Zeiss, Göttingen).

Quantification of sporozoite motility

Salivary glands of infected mosquitoes were isolated between days 17 and 25 after infection. They were kept in RPMI (supplemented with 50,000 units/l penicillin and 50 mg/l streptomycin) containing 3% bovine serum albumin (BSA, Roth) and transferred to a 96-well plate (Nunc MicroWell 96 well optical bottom plates, Sigma) for imaging. The plate was centrifuged for 5 min at 500 ***g*** to settle the sporozoites. DIC images were acquired at 0.33 Hz for 5 min. Sporozoite speeds were analyzed using the ImageJ plug-in 'Manual tracking' (Schneider et al., 2012).

Retrograde flow experiments

The retrograde flow experiments were performed on the self-built laser trap setup described in Quadt et al. (2016). In brief, beads (PC-S-2.0, streptavidin-polystyrene microparticles 1.5–1.9 µm, 1% w/v; Kisker) were held with minimal laser power by a stationary laser trap. Subsequently, the stage and the mounted self-built open flow cell containing gliding sporozoites were moved towards an optically trapped bead. The bead was then positioned onto the front end of the sporozoite. When sporozoite and bead made contact, the sporozoite pulled the bead out of the focus of the laser and translocated the bead to the rear of the cell. This was imaged with a frame rate of 100 images per second. The speeds of the transported beads were tracked using MATLAB routines (Quadt et al., 2016), which are available upon request.

Force measurements

The force measurement experiments were performed as described in detail in Quadt et al. (2016). Beads were captured in the center of the trap – this time with defined forces (70 pN, 130 pN and 190 pN) – and were brought in close proximity with the sporozoite until they touched the beads. Sporozoites were challenged to displace the bead from the focus of the trap.

Animal work

Generation of parasite lines and infections of mosquitoes was performed using female NMRI mice (Janvier). Monitoring of parasite prepatency and blood stage growth rates was performed using female C57BL/6 mice (Charles River). All animal experiments were performed according to the German Animal Welfare Act (Tierschutzgesetz) and were approved by the responsible German authorities (Regierungspräsidium Karlsruhe).

Acknowledgements

We thank M. Reinig for mosquito rearing and M. Streichfuss for introduction to laser tweezers. We are grateful to R. Douglas, T. Heinemann, K. Sadiq, P. Nandekar and J. Vahokoski for discussions and critically reading the manuscript. J.P.S., R.C.W., and F.F. are members of the CellNetworks cluster of Excellence at Heidelberg University. J.P.S. and F.F. are members of the Collaborative Research Center SFB 1129 of the German Research Foundation. F.F. was a member of the EU FP7 program EVIMalaR. C.A.M. was a member of the Hartmut Hoffman-Berling International Graduate School (HBIGS) and L.S. was a member of the Master Program Infectious Diseases at Heidelberg University.

Competing interests
The authors declare no competing or financial interests.

Author contributions
Conceptualization: C.A.M., H.P., R.C.W., I.K., F.F.; Methodology: C.A.M., K.A.Q., H.P., H.K., N.H.T., R.C.W., J.P.S., I.K.; Software: H.K., N.H.T., R.C.W.; Validation: C.A.M., K.A.Q., H.K.; Formal analysis: C.A.M., K.A.Q., H.P., L.S., R.C.W., I.K., F.F.; Investigation: C.A.M., K.A.Q., H.P., H.K., S.P.B., L.S.; Resources: J.P.S.; Data curation: C.A.M.; Writing - original draft: C.A.M., F.F.; Writing - review & editing: C.A.M., K.A.Q., H.P., N.H.T., R.C.W., J.P.S., I.K., F.F.; Visualization: C.A.M., K.A.Q., H.K.; Supervision: N.H.T., R.C.W., I.K., F.F.; Project administration: R.C.W., I.K., F.F.; Funding acquisition: N.H.T., R.C.W., J.P.S., I.K., F.F.

Funding
This work was funded by grant from the Chica and Heinz Schaller Foundation (Chica and Heinz Schaller-Stiftung; http://www.chs-stiftung.de), the Human Frontier Science Program RGY0071/2011 (http://www.hfsp.org) and the European Research Council StG 281719 (https://erc.europa.eu) to F.F.; the FRONTIER program of Heidelberg University (Universität Heidelberg; http://www.uni-heidelberg. de/exzellenzinitiative/zukunftskonzept/frontier_de. html) to R.C.W.; the Deutsche Forschungsgemeinschaft (DFG, German Research Foundation) – Projektnummer 240245660 - SFB 1129 (http://www.sfb1129.de) to J.S.P. and F.F.; the Academy of Finland grants 257537, 265112 and 292718 (http://www.aka.fi/en) and the Jane and Aatos Erkko Foundation (Jane ja Aatos Erkon Säätiö; http://jaes.fi/en/) to I.K.; the Sigrid Jusélius foundation (Sigrid Juséliuksen Säätiö; http://sigridjuselius.fi/en/foundation/) to S.P.B. and I.K.; the Emil Aaltonen Foundation (Emil Aaltosen Säätiö; http://www.emilaaltonen.fi) to H.P. and I.K.; the Burroughs Wellcome Fund (https://www.bwfund.org) to N.H.T. and the Klaus Tschira Foundation (Klaus Tschira Stiftung; http://www.klaus-tschira-stiftung.de) to R.C.W. The funders had no role in study design, data collection and analysis, decision to publish, or preparation of the manuscript.

Supplementary information
Supplementary information available online at
http://jcs.biologists.org/lookup/doi/10.1242/jcs.233775.supplemental

Peer review history
The peer review history is available online at
https://jcs.biologists.org/lookup/doi/10.1242/jcs.233755.reviewer-comments.pdf

References

Amino, R., Thiberge, S., Martin, B., Celli, S., Shorte, S., Frischknecht, F. and Ménard, R. (2006). Quantitative imaging of plasmodium transmission from mosquito to mammal. *Nat. Med.* **12**, 220-224. doi:10.1038/nm1350

Amino, R., Giovannini, D., Thiberge, S., Gueirard, P., Boisson, B., Dubremetz, J.-F., Prévost, M.-C., Ishino, T., Yuda, M. and Ménard, R. (2008). Host cell traversal is important for progression of the malaria parasite through the dermis to the liver. *Cell Host Microbe* **3**, 88-96. doi:10.1016/j.chom.2007.12.007

Andenmatten, N., Egarter, S., Jackson, A. J., Jullien, N., Herman, J.-P. and Meissner, M. (2013). Conditional genome engineering in toxoplasma gondii uncovers alternative invasion mechanisms. *Nat. Methods* **10**, 125-127. doi:10.1038/nmeth.2301

Aurrecoechea, C., Brestelli, J., Brunk, B. P., Dommer, J., Fischer, S., Gajria, B., Gao, X., Gingle, A., Grant, G., Harb, O. S. et al. (2009). Plasmodb: A functional genomic database for malaria parasites. *Nucleic Acids Res.* **37**, D539-D543. doi:10.1093/nar/gkn814

Bane, K. S., Lepper, S., Kehrer, J., Sattler, J. M., Singer, M., Reinig, M., Klug, D., Heiss, K., Baum, J., Mueller, A.-K. et al. (2016). The actin filament-binding protein coronin regulates motility in plasmodium sporozoites. *PLoS Pathog.* **12**, e1005710. doi:10.1371/journal.ppat.1005710

Bergman, L. W., Kaiser, K., Fujioka, H., Coppens, I., Daly, T. M., Fox, S., Matuschewski, K., Nussenzweig, V. and Kappe, S. H. (2003). Myosin a tail domain interacting protein (mtip) localizes to the inner membrane complex of plasmodium sporozoites. *J. Cell Sci.* **116**, 39-49. doi:10.1242/jcs.00194

Berman, H. M., Westbrook, J., Feng, Z., Gilliland, G., Bhat, T. N., Weissig, H., Shindyalov, I. N. and Bourne, P. E. (2000). The protein data bank. *Nucleic Acids Res.* **28**, 235-242. doi:10.1093/nar/28.1.235

Bhargav, S. P., Vahokoski, J., Kallio, J. P., Torda, A. E., Kursula, P. and Kursula, I. (2015). Two independently folding units of plasmodium profilin suggest evolution via gene fusion. *Cell. Mol. Life Sci.* **72**, 4193-4203. doi:10.1007/s00018-015-1932-0

Cerutti, D. S., Swope, W. C., Rice, J. E. and Case, D. A. (2014). Ff14ipq: a self-consistent force field for condensed-phase simulations of proteins. *J. Chem. Theory Comput.* **10**, 4515-4534. doi:10.1021/ct500643c

Courtemanche, N. and Pollard, T. D. (2013). Interaction of profilin with the barbed end of actin filaments. *Biochemistry* **52**, 6456-6466. doi:10.1021/bi400682n

Dolinsky, T. J., Czodrowski, P., Li, H., Nielsen, J. E., Jensen, J. H., Klebe, G. and Baker, N. A. (2007). Pdb2pqr: Expanding and upgrading automated preparation of biomolecular structures for molecular simulations. *Nucleic Acids Res.* **35**, W522-W525. doi:10.1093/nar/gkm276

Douglas, R. G., Amino, R., Sinnis, P. and Frischknecht, F. (2015). Active migration and passive transport of malaria parasites. *Trends Parasitol.* **31**, 357-362. doi:10.1016/j.pt.2015.04.010

Douglas, R. G., Nandekar, P., Aktories, J.-E., Kumar, H., Weber, R., Sattler, J. M., Singer, M., Lepper, S., Sadiq, S. K., Wade, R. C. et al. (2018). Inter-subunit interactions drive divergent dynamics in mammalian and plasmodium actin filaments. *PLoS Biol.* **16**, e2005345. doi:10.1371/journal.pbio.2005345

Ferron, F., Rebowski, G., Lee, S. H. and Dominguez, R. (2007). Structural basis for the recruitment of profilin-actin complexes during filament elongation by ena/vasp. *EMBO J.* **26**, 4597-4606. doi:10.1038/sj.emboj.7601874

Frischknecht, F. and Matuschewski, K. (2017). Plasmodium sporozoite biology. *Cold Spring Harb. Perspect. Med.* **7**, a025478. doi:10.1101/cshperspect.a025478

Frischknecht, F., Baldacci, P., Martin, B., Zimmer, C., Thiberge, S., Olivo-Marin, J.-C., Shorte, S. L. and Ménard, R. (2004). Imaging movement of malaria parasites during transmission by anopheles mosquitoes. *Cell. Microbiol.* **6**, 687-694. doi:10.1111/j.1462-5822.2004.00395.x

Frischknecht, F., Martin, B., Thiery, I., Bourgouin, C. and Menard, R. (2006). Using green fluorescent malaria parasites to screen for permissive vector mosquitoes. *Malar. J.* **5**, 23. doi:10.1186/1475-2875-5-23

Gras, S., Jimenez-Ruiz, E., Klinger, C. M., Schneider, K., Klingl, A., Lemgruber, L. and Meissner, M. (2019). An endocytic-secretory cycle participates in toxoplasma gondii in motility. *PLoS Biol.* **17**, e3000060. doi:10.1371/journal.pbio.3000060

Hegge, S., Münter, S., Steinbüchel, M., Heiss, K., Engel, U., Matuschewski, K. and Frischknecht, F. (2010). Multistep adhesion of plasmodium sporozoites. *FASEB J.* **24**, 2222-2234. doi:10.1096/fj.09-148700

Hegge, S., Uhrig, K., Streichfuss, M., Kynast-Wolf, G., Matuschewski, K., Spatz, J. P. and Frischknecht, F. (2012). Direct manipulation of malaria parasites with optical tweezers reveals distinct functions of plasmodium surface proteins. *ACS Nano* **6**, 4648-4662. doi:10.1021/nn203616u

Heintzelman, M. B. (2015). Gliding motility in apicomplexan parasites. *Semin. Cell Dev. Biol.* **46**, 135-142. doi:10.1016/j.semcdb.2015.09.020

Hellmann, J. K., Münter, S., Kudryashev, M., Schulz, S., Heiss, K., Müller, A.-K., Matuschewski, K., Spatz, J. P., Schwarz, U. S. and Frischknecht, F. (2011). Environmental constraints guide migration of malaria parasites during transmission. *PLoS Pathog.* **7**, e1002080. doi:10.1371/journal.ppat.1002080

Hopp, C. S., Chiou, K., Ragheb, D. R. T., Salman, A. M., Khan, S. M., Liu, A. J. and Sinnis, P. (2015). Longitudinal analysis of plasmodium sporozoite motility in the dermis reveals component of blood vessel recognition. *eLife* **4**, e07789. doi:10.7554/eLife.07789.025

Ignatev, A., Bhargav, S. P., Vahokoski, J., Kursula, P. and Kursula, I. (2012). The lasso segment is required for functional dimerization of the plasmodium formin 1 fh2 domain. *PLoS ONE* **7**, e33586. doi:10.1371/journal.pone.0033586

Jacot, D., Tosetti, N., Pires, I., Stock, J., Graindorge, A., Hung, Y.-F., Han, H., Tewari, R., Kursula, I. and Soldati-Favre, D. (2016). An apicomplexan actin-binding protein serves as a connector and lipid sensor to coordinate motility and invasion. *Cell Host Microbe* **20**, 731-743. doi:10.1016/j.chom.2016.10.020

Janse, C. J., Ramesar, J. and Waters, A. P. (2006). High-efficiency transfection and drug selection of genetically transformed blood stages of the rodent malaria parasite plasmodium berghei. *Nat. Protoc.* **1**, 346-356. doi:10.1038/nprot.2006.53

Kehrer, J., Frischknecht, F. and Mair, G. R. (2016). Proteomic analysis of the plasmodium berghei gametocyte egressome and vesicular bioid of osmiophilic body proteins identifies merozoite trap-like protein (mtrap) as an essential factor for parasite transmission. *Mol. Cell. Proteomics* **15**, 2852-2862. doi:10.1074/mcp.M116.058263

Khater, E. I., Sinden, R. E. and Dessens, J. T. (2004). A malaria membrane skeletal protein is essential for normal morphogenesis, motility, and infectivity of sporozoites. *J. Cell Biol.* **167**, 425-432. doi:10.1083/jcb.200406068

Klug, D. and Frischknecht, F. (2017). Motility precedes egress of malaria parasites from oocysts. *eLife* **6**, e19157. doi:10.7554/eLife.19157

Klug, D., Mair, G. R., Frischknecht, F. and Douglas, R. G. (2016). A small mitochondrial protein present in myzozoans is essential for malaria transmission. *Open Biol* **6**, 160034. doi:10.1098/rsob.160034

Kursula, I., Kursula, P., Ganter, M., Panjikar, S., Matuschewski, K. and Schüler, H. (2008). Structural basis for parasite-specific functions of the divergent profilin of plasmodium falciparum. *Structure* **16**, 1638-1648. doi:10.1016/j.str.2008.09.008

Lehmann, C., Heitmann, A., Mishra, S., Burda, P.-C., Singer, M., Prado, M., Niklaus, L., Lacroix, C., Ménard, R., Frischknecht, F. et al. (2014). A cysteine protease inhibitor of plasmodium berghei is essential for exo-erythrocytic development. *PLoS Pathog.* **10**, e1004336. doi:10.1371/journal.ppat.1004336

Meagher, K. L., Redman, L. T. and Carlson, H. A. (2003). Development of polyphosphate parameters for use with the amber force field. *J. Comput. Chem.* **24**, 1016-1025. doi:10.1002/jcc.10262

Mehta, S. and Sibley, L. D. (2011). Actin depolymerizing factor controls actin turnover and gliding motility in toxoplasma gondii. *Mol. Biol. Cell* **22**, 1290-1299. doi:10.1091/mbc.e10-12-0939

Meissner, M., Schluter, D. and Soldati, D. (2002). Role of toxoplasma gondii myosin a in powering parasite gliding and host cell invasion. *Science* **298**, 837-840. doi:10.1126/science.1074553

Meissner, M., Ferguson, D. J. P. and Frischknecht, F. (2013). Invasion factors of apicomplexan parasites: Essential or redundant? *Curr. Opin. Microbiol.* **16**, 438-444. doi:10.1016/j.mib.2013.05.002

Ménard, R., Tavares, J., Cockburn, I., Markus, M., Zavala, F. and Amino, R. (2013). Looking under the skin: the first steps in malarial infection and immunity. *Nat. Rev. Microbiol.* **11**, 701-712. doi:10.1038/nrmicro3111

Moll, K., Ljungström, I., Perlman, H., Scherf, A. and Wahlgren, M. (2008). *Methods in Malaria Research*, 5th edn. Manassas, VA: MR4/ATCC; Paris, France.

Moreau, C. A., Bhargav, S. P., Kumar, H., Quadt, K. A., Piirainen, H., Strauss, L., Kehrer, J., Streichfuss, M., Spatz, J. P., Wade, R. C. et al. (2017). A unique profilin-actin interface is important for malaria parasite motility. *PLoS Pathog.* **13**, e1006412. doi:10.1371/journal.ppat.1006412

Münter, S., Sabass, B., Selhuber-Unkel, C., Kudryashev, M., Hegge, S., Engel, U., Spatz, J. P., Matuschewski, K., Schwarz, U. S. and Frischknecht, F. (2009). Plasmodium sporozoite motility is modulated by the turnover of discrete adhesion sites. *Cell Host Microbe* **6**, 551-562. doi:10.1016/j.chom.2009.11.007

Pardee, J. D. and Spudich, J. A. (1982). Purification of muscle actin. *Methods Cell Biol.* **24**, 271-289. doi:10.1016/S0091-679X(08)60661-5

Pimenta, P. F., Touray, M. and Miller, L. (1994). The journey of malaria sporozoites in the mosquito salivary gland. *J. Eukaryot. Microbiol.* **41**, 608-624. doi:10.1111/j.1550-7408.1994.tb01523.x

Price, D. J. and Brooks, C. L.III. (2004). A modified tip3p water potential for simulation with Ewald summation. *J. Chem. Phys.* **121**, 10096-10103. doi:10.1063/1.1808117

Prudêncio, M., Rodriguez, A. and Mota, M. M. (2006). The silent path to thousands of merozoites: the plasmodium liver stage. *Nat. Rev. Microbiol.* **4**, 849-856. doi:10.1038/nrmicro1529

Quadt, K. A., Streichfuss, M., Moreau, C. A., Spatz, J. P. and Frischknecht, F. (2016). Coupling of retrograde flow to force production during malaria parasite migration. *ACS Nano* **10**, 2091-2102. doi:10.1021/acsnano.5b06417

Ryckaert, J.-P., Ciccotti, G. and Berendsen, H. J. C. (1977). Numerical-integration of the cartesian equations of motion of a system with constraints: molecular dynamics of n-alkanes. *J. Comput. Physics* **23**, 327-341. doi:10.1016/0021-9991(77)90098-5

Santos, J. M., Egarter, S., Zuzarte-Luis, V., Kumar, H., Moreau, C. A., Kehrer, J., Pinto, A., da Costa, M., Franke-Fayard, B. et al. (2017). Malaria parasite LIMP protein regulates sporozoite gliding motility and infectivity in mosquito and mammalian hosts. *eLife* **6** e24109. doi:10.7554/eLife.24109

Sato, Y., Hliscs, M., Dunst, J., Goosmann, C., Brinkmann, V., Montagna, G. N. and Matuschewski, K. (2016). Comparative plasmodium gene overexpression reveals distinct perturbation of sporozoite transmission by profilin. *Mol. Biol. Cell* **27**, 2234-2244. doi:10.1091/mbc.E15-10-0734

Schneider, C. A., Rasband, W. S. and Eliceiri, K. W. (2012). Nih image to imagej: 25 years of image analysis. *Nat. Methods* **9**, 671-675. doi:10.1038/nmeth.2089

Silvie, O., Goetz, K. and Matuschewski, K. (2008). A sporozoite asparagine-rich protein controls initiation of plasmodium liver stage development. *PLoS Pathog.* **4**, e10000086. doi:10.1371/journal.ppat.1000086

Skillman, K. M., Diraviyam, K., Khan, A., Tang, K., Sept, D. and Sibley, L. D. (2011). Evolutionarily divergent, unstable filamentous actin is essential for gliding motility in apicomplexan parasites. *PLoS Pathog.* **7**, e1002280. doi:10.1371/journal.ppat.1002280

Skillman, K. M., Daher, W., Ma, C. I., Soldati-Favre, D. and Sibley, L. D. (2012). Toxoplasma gondii profilin acts primarily to sequester g-actin while formins efficiently nucleate actin filament formation in vitro. *Biochemistry* **51**, 2486-2495. doi:10.1021/bi201704y

Spaccapelo, R., Janse, C. J., Caterbi, S., Franke-Fayard, B., Bonilla, J. A., Syphard, L. M., Di Cristina, M., Dottorini, T., Savarino, A., Cassone, A. et al. (2010). Plasmepsin 4-deficient plasmodium berghei are virulence attenuated and induce protective immunity against experimental malaria. *Am. J. Pathol.* **176**, 205-217. doi:10.2353/ajpath.2010.090504

Spreng, B., Fleckenstein, H., Kübler, P., Di Biagio, C., Benz, M., Patra, P., Schwarz, U. S., Cyrklaff, M. and Frischknecht, F. (2019). Microtubule number and length determine cellular shape and function in plasmodium. *EMBO J.* **38**, e100984. doi:10.15252/embj.2018100984

Steel, R. W. J., Pei, Y., Camargo, N., Kaushansky, A., Dankwa, D. A., Martinson, T., Nguyen, T., Betz, W., Cardamone, H., Vigdorovich, V. et al. (2018). Plasmodium yoelii s4/celtos is important for sporozoite gliding motility and cell traversal. *Cell. Microbiol.* **20**, e12817. doi:10.1111/cmi.12817

Sultan, A. A., Thathy, V., Frevert, U., Robson, K. J. H., Crisanti, A., Nussenzweig, V., Nussenzweig, R. S. and Ménard, R. (1997). Trap is necessary for gliding motility and infectivity of plasmodium sporozoites. *Cell* **90**, 511-522. doi:10.1016/S0092-8674(00)80511-5

Tardieux, I. and Baum, J. (2016). Reassessing the mechanics of parasite motility and host-cell invasion. *J. Cell Biol.* **214**, 507-515. doi:10.1083/jcb.201605100

Tavares, J., Formaglio, P., Thiberge, S., Mordelet, E., Van Rooijen, N., Medvinsky, A., Ménard, R. and Amino, R. (2013). Role of host cell traversal by the malaria sporozoite during liver infection. *J. Exp. Med.* **210**, 905-915. doi:10.1084/jem.20121130

Vahokoski, J., Bhargav, S. P., Desfosses, A., Andreadaki, M., Kumpula, E.-P., Martinez, S. M., Ignatev, A., Lepper, S., Frischknecht, F., Sidén-Kiamos, I. et al. (2014). Structural differences explain diverse functions of plasmodium actins. *PLoS Pathog.* **10**, e1004091. doi:10.1371/journal.ppat.1004091

Volkmann, K., Pfander, C., Burstroem, C., Ahras, M., Goulding, D., Rayner, J. C., Frischknecht, F., Billker, O. and Brochet, M. (2012). The alveolin imc1h is required for normal ookinete and sporozoite motility behaviour and host colonisation in plasmodium berghei. *PLoS ONE* **7**, e41409. doi:10.1371/journal.pone.0041409

Wang, J., Wolf, R. M., Caldwell, J. W., Kollman, P. A. and Case, D. A. (2004). Development and testing of a general amber force field. *J. Comput. Chem.* **25**, 1157-1174. doi:10.1002/jcc.20035